ADVANCES IN ATMOSPHERIC SCIENCES, VOL. 39, APRIL 2022, 576–590

• **Original Paper** •

Influence of Major Stratospheric Sudden Warming on the Unprecedented Cold Wave in East Asia in January 2021※

Yingxian ZHANG[1], Dong SI*[2], Yihui DING[1], Dabang JIANG[2], Qingquan LI[1], and Guofu WANG[1]

[1]*National Climate Center*, *China Meteorological Administration*, *Beijing* 100081, *China*

[2]*Climate Change Research Center*, *Institute of Atmospheric Physics*, *Chinese Academy of Sciences*, *Beijing* 100029, *China*

(Received 27 August 2021; revised 31 December 2021; accepted 18 January 2022)

ABSTRACT

An unprecedented cold wave intruded into East Asia in early January 2021 and led to record-breaking or historical extreme low temperatures over vast regions. This study shows that a major stratospheric sudden warming (SSW) event at the beginning of January 2021 exerted an important influence on this cold wave. The major SSW event occurred on 2 January 2021 and subsequently led to the displacement of the stratospheric polar vortex to the East Asian side. Moreover, the SSW event induced the stratospheric warming signal to propagate downward to the mid-to-lower troposphere, which not only enhanced the blocking in the Urals–Siberia region and the negative phase of the Arctic Oscillation, but also shifted the tropospheric polar vortex off the pole. The displaced tropospheric polar vortex, Ural blocking, and another downstream blocking ridge over western North America formed a distinct inverted omega-shaped circulation pattern (IOCP) in the East Asia–North Pacific sector. This IOCP was the most direct and impactful atmospheric pattern causing the cold wave in East Asia. The IOCP triggered a meridional cell with an upward branch in East Asia and a downward branch in Siberia. The meridional cell intensified the Siberian high and low-level northerly winds, which also favored the invasion of the cold wave into East Asia. Hence, the SSW event and tropospheric circulations such as the IOCP, negative phase of Arctic Oscillation, Ural blocking, enhanced Siberian high, and eastward propagation of Rossby wave eventually induced the outbreak of an unprecedented cold wave in East Asia in early January 2021.

Key words: cold wave, stratospheric sudden warming, polar vortex, Ural blocking, Siberian high

Citation: Zhang, Y. X., D. Si, Y. H. Ding, D. B. Jiang, Q. Q. Li, and G. F. Wang, 2022: Influence of major stratospheric sudden warming on the unprecedented cold wave in East Asia in January 2021. *Adv. Atmos. Sci.*, **39**(4), 576–590, https://doi.org/10.1007/s00376-022-1318-9.

Article Highlights:

- A major stratospheric sudden warming (SSW) event occurred at the beginning of January 2021.
- The major SSW event exerted an important influence on the cold wave in East Asia in early January 2021.
- The SSW event, IOCP, negative Arctic oscillation, and enhanced Ural blocking/Siberian high eventually induced the cold wave in East Asia in early January 2021.

1. Introduction

Cold events have become more intense and frequent in East Asian winters since the beginning of the twenty-first century. A series of extreme cold events occurred in East Asia in the winters of 2004/05 (Ding and Ma, 2008), 2007/08 (Wu et al., 2011; Zhou et al., 2011; Kuang et al., 2019), 2009/10 (Hori et al., 2011), and 2015/16 (Ma and Zhu, 2019; Dai and Mu, 2020). The frequent occurrence of extreme cold events is of great concern for adaptation to a warmer world (Kuang et al., 2019). The impressive cold surges in the early winter of 2020/21, which led to record-breaking low temperatures in central and eastern China, aroused widespread public concern (Dai et al., 2021; Zhang et al., 2021a; Zheng et al., 2021; Bueh et al., 2022; Yao et al., 2022). These extreme low temperatures are often transnational or even continental, while it is relatively mild in the Arctic region. This distinct temperature pattern is referred to as the "cold continents and warm Arctic" (Overland et al., 2011; Luo et al., 2016).

Regional extreme low-temperature events (RELTEs) have been studied as a result of their long duration and large area of influence. Winter RELTEs are usually accompanied

※ This paper is a contribution to the special issue on Extreme Cold Events from East Asia to North America in Winter 2020/21.

* Corresponding author: Dong SI
Email: sidong@mail.iap.ac.cn

by strong cold surges, heavy snow, and freezing disasters. Many case studies have therefore focused on the outbreak of RELTEs, their mechanisms of development, and their possible causes (Chen et al., 2002; Ding and Ma, 2008; Wu et al., 2017). Intensification of the blocking high in the Ural Mountains or Siberia, accompanied by a deepened East Asian trough, is typical of many winter RELTEs (Ding et al., 2008; Tao and Wei, 2008; Wen et al., 2009; Zhou et al., 2009; Zuo et al., 2015). A collapse of the blocking pattern over Eurasia and the Atlantic can induce an outbreak of cold air in East Asia (Tao, 1957). Winter RELTEs in Eurasia can also be manifested by the abrupt expansion or enhancement of the Siberian high. The intraseasonal variation of the Siberian high is considered to be a critical factor in the occurrence of cold waves (Ding and Krishnamurti, 1987; Gong and Ho, 2002; Takaya and Nakamura, 2005a, b; Park et al., 2008). Moreover, previous studies also have analyzed the influence of the Arctic Oscillation (Thompson and Wallace, 1998; Jeong and Ho, 2005; Wang and Chen, 2010) and Arctic sea ice (Honda et al., 2009; Petoukhov and Semenov, 2010; Wu et al., 2015) on the occurrence of cold surges in Eurasia.

Both observational studies (Yu et al., 2018) and model simulations (Gillett and Thompson, 2003; Charlton et al., 2004) have provided robust evidence that the state of the stratosphere can influence atmospheric circulation in the troposphere. Stratospheric sudden warming (SSW) is the clearest and strongest manifestation of the coupling between the stratospheric and tropospheric systems (Charlton and Polvani, 2007). It has been shown that the cold events over Europe and East Asia in winter can be attributed to the occurrence of SSW (Scaife and Knight, 2008; Lü et al., 2020; Yu et al., 2022). The displacement or splitting of the stratospheric polar vortex during a major SSW event may lead to different patterns of surface weather and climate anomalies (Mitchell et al., 2013). The dynamic influence of the stratosphere is known to play a part in shaping the circulation patterns of the troposphere in winter (Davini et al., 2014).

Three outbreaks of cold air occurred in China in the early winter of 2020/21 on 13–15 December 2020, 29 December 2020–1 January 2021, and 6–8 January 2021 (Dai et al., 2021; Zheng et al., 2021). These three cold air events were related to three RELTEs in Eurasia. The latter two events were categorized as the cold surge level, and the third event is popularly referred to as the "boss level". The boss level cold wave swept through vast areas of China. Beijing faced a minimum temperature of –19.6°C on 7 January 2021, the coldest temperature since 1966. The synergistic effect of the warm Arctic and the cold tropical Pacific Ocean (i.e., La Niña) was considered to have contributed to the cold winter of 2020/21 by providing a background for the intensification of the atmospheric circulation anomalies at mid-to-high latitudes (Zheng et al., 2021). However, the effects of the stratosphere on this cold wave are not clear. More importantly, it is not known why the third cold wave from 6–8 January 2021 was so intense. We therefore carried out a comprehensive analysis of this cold wave to investigate the possible influence from the stratosphere.

This paper is organized as follows. Section 2 describes the datasets and methods. Section 3 analyzes the SSW event in early January 2021 and its impacts on the extreme cold wave in East Asia. Section 4 summarizes our results.

2. Data and methods

2.1. *Data*

We used atmospheric data from the National Centers for Environmental Prediction and the National Center for Atmospheric Research reanalysis dataset with a temporal resolution of 24 h and a horizontal resolution of 2.5° × 2.5° (Kalnay et al., 1996). The variables included the geopotential height, the zonal and meridional wind components, the vertical p-velocity, the temperature, and the sea level pressure. The reanalysis data of daily minimum surface air temperature at 2 m with a horizontal resolution of roughly 1.9° × 1.9° from 1948 to 2021 was used to objectively identify the RELTE events.

The gauge-based observational daily minimum air temperature dataset was from version 3.0 of the basic historical meteorological dataset of a dense national network released by the National Meteorological Information Center of the China Meteorological Administration. The total number of national stations was 2479, and all the daily data used here had been subjected to quality control procedures by the National Meteorological Information Center. The observed extreme low temperatures from 6–8 January 2021 were derived from the Meteorological Disaster Risk Management System developed by the National Climate Center of the China Meteorological Administration. In the Meteorological Disaster Risk Management System, the lowest and second lowest values of daily minimum temperature for each baseline year (the baseline is 1981–2010) are chosen as the sample set. All temperatures in the sample set are sorted in ascending order, and the 5th percentile value is defined as the historical extreme value. The Meteorological Disaster Risk Management System outputs information from qualified sites at which the daily minimum temperatures reach historical extreme values or break low-temperature records.

2.2. *Methods*

2.2.1. *Objective identification of the RELTE in East Asia*

An objective method was used to identify the RELTEs in East Asia in early January 2021. This method was put forward by Ren et al. (2012) and developed by Zhang et al. (2021b) to identify RELTEs based on a gridded dataset. An RELTE was identified via a two-step process. First, an extreme low temperature in each grid was identified if the minimum temperature fell below the extreme low-temperature threshold— that is, the 10th percentile of its distribution defined by five consecutive days in winter (December–

January–February) from 1948/49 to 2020/21 centered on a given day. Second, one potential RELTE event was identified by considering the spatiotemporal continuum of extreme low temperatures. The spatial extent of one extreme low-temperature zone (i.e., spatial continuum) on one given day involved all the grids and their neighbors in which the minimum temperatures fell below the extreme low-temperature threshold. It was assumed that one RELTE continued (i.e., temporal continuum) if the event overlapped with any new extreme low-temperature zone in the downstream area on the following day. A detailed introduction to this method is given by Zhang et al. (2021b).

2.2.2. *Calculations of the Siberian high and Arctic Oscillation index*

The Siberian high index was defined as the averaged sea level pressure over the region (40°–60°N, 80°–120°E), which is used by the Chinese National Climate Center to monitor the Siberian high. The Arctic Oscillation index was obtained from the National Oceanic and Atmospheric Administration Climate Prediction Center (https://www.cpc.ncep.noaa.gov/products/precip/CWlink/daily_ao_index/ao.shtml).

2.2.3. *Calculation of the Eliassen–Palm flux*

We examined the Eliassen–Palm flux and its divergence (Edmon et al., 1980), which depict planetary wave activity and eddy forcing on the zonal-mean flow, to determine the influence of wave activity in the troposphere on the stratospheric circulation. The Eliassen–Palm flux vectors were defined as:

$$\left\{F_\varphi, F_p\right\} = \{-a\cos\varphi\overline{u'v'}, fa\cos\varphi\frac{\overline{v'\theta'}}{\bar{\theta}_p}\}, \tag{1}$$

where a is the radius of the Earth, φ is the latitude, $f = 2\omega\sin\varphi$ is the Coriolis parameter with ω indicating the rotational angular velocity of the Earth, u, v are the zonal and meridional winds, θ is the potential temperature, and p is the pressure level. The overbars, primes, and subscripts on the right side of Eq. (1) denote the zonal means, departures, and partial differentiation, respectively. The divergence of the Eliassen–Palm flux is given by:

$$\nabla\cdot\boldsymbol{F} = \frac{1}{a\cos\varphi}\frac{\partial\left(F_\varphi\cos\varphi\right)}{\partial\varphi} + \frac{\partial F_p}{\partial p}. \tag{2}$$

To give a graphical display in latitude–pressure coordinates, the Eliassen–Palm flux vectors were scaled by the scaling factors:

$$\left\{\bar{F}_\varphi, \bar{F}_p\right\} = \cos\varphi\{\frac{1}{a}\frac{F_\varphi}{S_\varphi}, \frac{F_p}{S_p}\}, \tag{3}$$

where $S_\varphi = \pi$ and $S_p = 10^5$(Pa) are the scale factors. The Eliassen–Palm flux divergence was not scaled. Using this method, the values of divergence at a given point on a graph represent the tendency in the angular momentum per unit mass.

2.2.4. *Calculation of Takaya–Nakamura flux*

To examine the stationary Rossby wave propagation associated with the cold wave, the wave activity flux formulated by Takaya and Nakamura (2001) (hereafter TN flux) was used in this study. The horizontal flux components were defined as:

$$\boldsymbol{W} = \frac{p\cos\varphi}{2|\boldsymbol{U}|}\begin{Bmatrix} \frac{U}{a^2\cos^2\varphi}\left[\left(\frac{\partial\psi'}{\partial\lambda}\right)^2 - \psi'\frac{\partial^2\psi'}{\partial\lambda^2}\right] + \frac{V}{a^2\cos\varphi}\left[\frac{\partial\psi'}{\partial\lambda}\frac{\partial\psi'}{\partial\varphi} - \psi'\frac{\partial^2\psi'}{\partial\lambda\partial\varphi}\right] \\ \frac{U}{a^2\cos\varphi}\left[\frac{\partial\psi'}{\partial\lambda}\frac{\partial\psi'}{\partial\varphi} - \psi'\frac{\partial^2\psi'}{\partial\lambda\partial\varphi}\right] + \frac{V}{a^2}\left[\left(\frac{\partial\psi'}{\partial\varphi}\right)^2 - \psi'\frac{\partial^2\psi'}{\partial\varphi^2}\right] \end{Bmatrix}, \tag{4}$$

where a, φ, and λ denote the radius of the Earth, latitude, and longitude, respectively, ψ' is the perturbation geostrophic stream function; $\boldsymbol{U}$, U and V are the horizontal basic flow velocity and the zonal and meridional components, respectively, and p is the pressure level.

3. Results

3.1. *The extreme cold event in early January 2021*

An RELTE was objectively identified in East Asia from 5–10 January 2021. Figure 1 shows that most regions of China, apart from Tibet and Southwest and Northeast China, were affected by this RELTE, especially from 6–8 January. In addition, this RELTE also affected other parts of East Asia, including Mongolia, the Korean Peninsula, and Japan.

This cold wave had an enormous impact. The lowest temperatures across almost all of China dropped below 0°C, and they were even below –28°C in Inner Mongolia and Northeast China. The 0°C isotherm moved south to 25°N during the period of 6–8 January 2021 (Fig. 2a). As a result, 383 stations, mainly located in eastern China and north of the Yangtze River, broke their low-temperature records (56 stations) or reached historical extreme values (327 stations) (Fig. 2b). The daily minimum temperature averaged over these stations decreased after 28 December 2020 (Fig. 2c). When the cold wave occurred, the minimum temperature decreased dramatically and reached a minimum of –17.7°C (12°C lower than the climatology) on 7 January 2021.

3.2. *The SSW event and its possible cause*

A prominent SSW event occurred at the beginning of January 2021 before the extreme cold wave. Following the World Meteorological Organization definition (Andrews et al., 1987; Krüger et al., 2005), a major SSW event occurs when the 10-hPa zonal-mean zonal winds at 60°N become easterly and the 10-hPa zonal-mean temperature gradient between 90°N and 60°N becomes positive. Figure 3a shows that the 10-hPa zonal-mean temperature gradient between

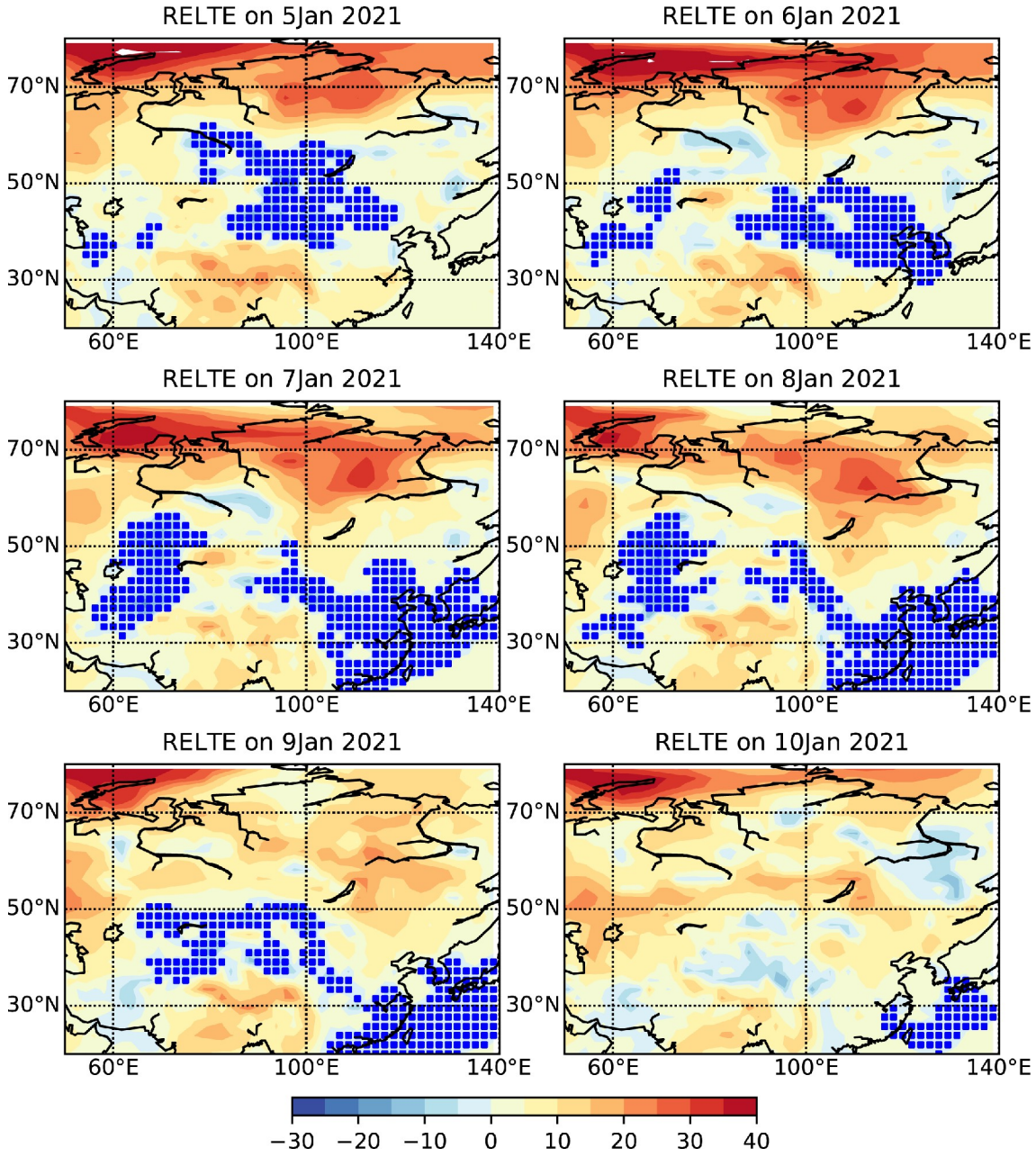

Fig. 1. Spatiotemporal evaluation of the RELTE in East Asia from 5 to 10 January 2021. The color shading shows the daily minimum temperature anomaly relative to the extreme low-temperature thresholds (units: °C). The blue dots indicate the regions affected by this event where daily minimum temperatures fell below the extreme low-temperature thresholds defined in section 2.2.1.

90°N and 60°N was negative in December 2020, changed from negative to positive on 2 January 2021, and reached a maximum on 6 January 2021. In addition, the 10-hPa zonal-mean zonal wind at 60°N changed from westerly to easterly on 5 January 2021 (Fig. 3b). Based on the World Meteorological Organization definition, this SSW event can be categorized as a major event. Figure 3c shows the temporal evolution of the cross section of the temperature and zonal winds over the polar cap. Warming with easterly winds occurred at 10 hPa at the end of December 2020 and then propagated rapidly downward into the lower stratosphere and upper troposphere within about one week.

This major SSW event persisted for about two weeks until 19 January 2021. The potential vorticity (PV) in the lower and midstratosphere in the Arctic decreased rapidly as a result of the SSW event. The PV at 10 hPa decreased from >200 PVU (PVU is potential vorticity units in 10^{-6} m^2 kg^{-1} s^{-1}) to 150–200 PVU after 5 January (Fig. 3d). According to the criterion proposed by Charlton and Polvani (2007), this SSW event was classified as a vortex displacement event. The center of the stratospheric polar vortex clearly shifted off the pole, and the distortion of the polar vortex was characterized by an "anti-comma shape" (Fig. 3e). The tail of the anti-comma-shape stratospheric polar vortex

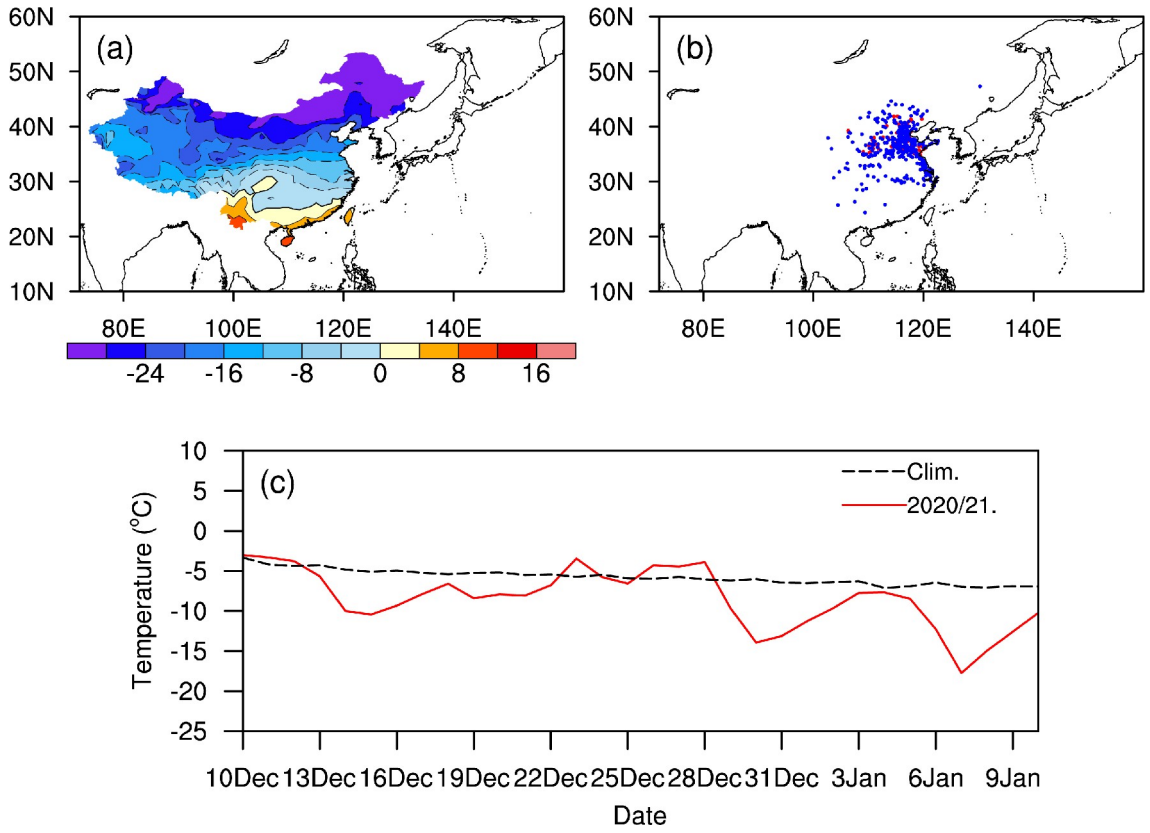

Fig. 2. (a) Distribution of the minimum value of the daily minimum temperature (units: °C) over China from 6 to 8 January 2021. (b) Sites at which the daily minimum temperature broke records (red dots) or reached historical extreme values (blue dots) over China from 6 to 8 January 2021. (c) Daily variation of the minimum temperature (units: °C) averaged for the 383 stations shown in Figure (b) from 10 December 2020 to 10 January 2021 (red line) and its climatology for the time period 1981–2010 (black dashed line).

moved toward East Asia and decreased the geopotential height there, which favored movement of the cold air mass out of the Arctic Circle and downward into East Asia. During the SSW event, the stratospheric geopotential height increased around the North Pole and decreased over East Asia compared to the climatology (Fig. 3e).

The SSW event and displacement of the stratospheric polar vortex may be attributed to the increase in the poleward transient eddy heat transport in the troposphere. A poleward propagating Rossby wave on 26–28 December 2020 resulted in a heat intrusion from the North Atlantic into the Arctic region (Zhang et al., 2021a). The poleward heat intrusion excited a strong tropospheric Rossby wave propagating from the troposphere to the midstratosphere in late December 2020 (Fig. 4a), which led to the stratospheric warming and high-pressure anomalies in the Arctic region. On 1 January 2021, the stratospheric warming and high pressure emerged around the Chukchi Sea and East Siberian Sea, then moved westward toward the Kara Sea on 3 January 2021 (Fig. A1 in the Appendix). Hence, the westward movement of the midstratospheric high pressure squeezed the polar vortex toward the East Asian side.

Previous studies have revealed relationships between the tropospheric planetary wave pattern and SSW events (Nakagawa and Yamazaki, 2006) and the horizontal distribution of the stratospheric polar vortex (Liu and Zhang, 2014), respectively. Before the SSW event in early January 2021, the Eliassen–Palm flux was clearly upward into the midstratosphere over the region 40°–60°N and the planetary wave propagated equatorward when entering the midstratosphere (Fig. 4a). The Eliassen–Palm flux diverged from 10 hPa to 30 hPa above the Arctic region, but converged at midlatitudes, indicating an acceleration of the basic westerly flow in the Arctic. From 2 to 5 January 2021, the upward planetary wave propagated poleward in the mid-to-lower stratosphere and converged at high latitudes and in the Arctic region (Fig. 4b). This favored a deceleration of the basic westerly flow and a transition from a westerly to an easterly flow. In addition, the tropospheric planetary wave can induce poleward eddy heat flux, which triggers a warming tendency at higher latitudes and cooling at lower latitudes – that is, an SSW event (Matsuno, 1971).

3.3. *The impacts of the SSW event on the tropospheric circulation*

To reveal the impacts of SSW on the atmospheric circulation in the troposphere, Fig. 5a shows the height–time cross section of the geopotential height anomalies averaged over the polar cap. The geopotential height anomalies in the midstratosphere were negative in December 2020. When the

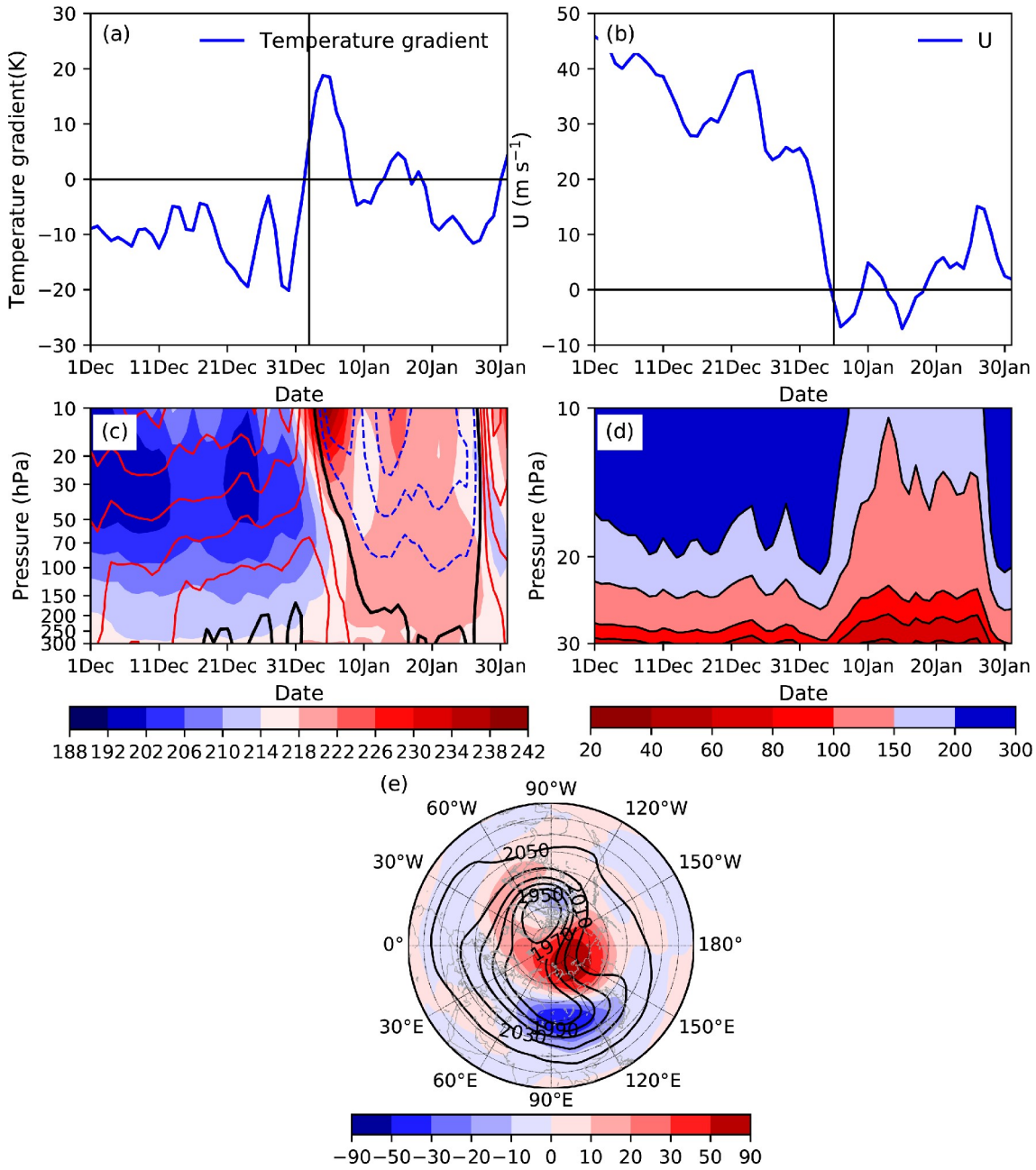

Fig. 3. (a) Temporal evolution of the 10-hPa zonal-mean temperature gradient (units: K) between 90°N and 60°N from 1 December 2020 to 31 January 2021. (b) Temporal evolution of the 10-hPa zonal-mean zonal wind at 60°N (units: m s^{-1}). (c) Time–height cross section of the temperature of the polar cap (65°–90°N) (shading; units: K) and zonal winds (contours; red/blue contours indicate positive/negative values and black contours indicate zero line; interval 5 m s^{-1}) from 1 December 2020 to 31 January 2021. (d) Time–height cross section of the potential vorticity (shading; units: PVU) over the polar region (75°–90°N). (e) Distribution of the geopotential height (contours; units: dagpm) and its anomalies (shading; units: dagpm) at 50 hPa averaged from 2 to 5 January 2021.

SSW event occurred at the beginning of January 2021, there were prominent downward propagating stratospheric signals of strong positive geopotential height anomalies over the polar cap. The downward propagation of the stratospheric signals reached the mid and lower troposphere at the high latitudes, which enhanced the negative phase of the Arctic Oscillation (Tomassini et al., 2012; Yu et al., 2022). It was reinforced and reached its lowest value on 5 January 2021 (Fig. 5b). The Siberian high was stronger than its climatology and strengthened after 5 January 2021 (Fig. 5c). Moreover, the associated downward propagation signal also contributed to the enhancement of the blocking over the Urals region (Lu and Ding, 2013). Figure 5d shows the time–height cross section of geopotential height anomaly averaged over 55°–75°N, 80°–110°E from 1 December 2020 to 31 January 2021. A prominent feature seen in Fig. 5d is the

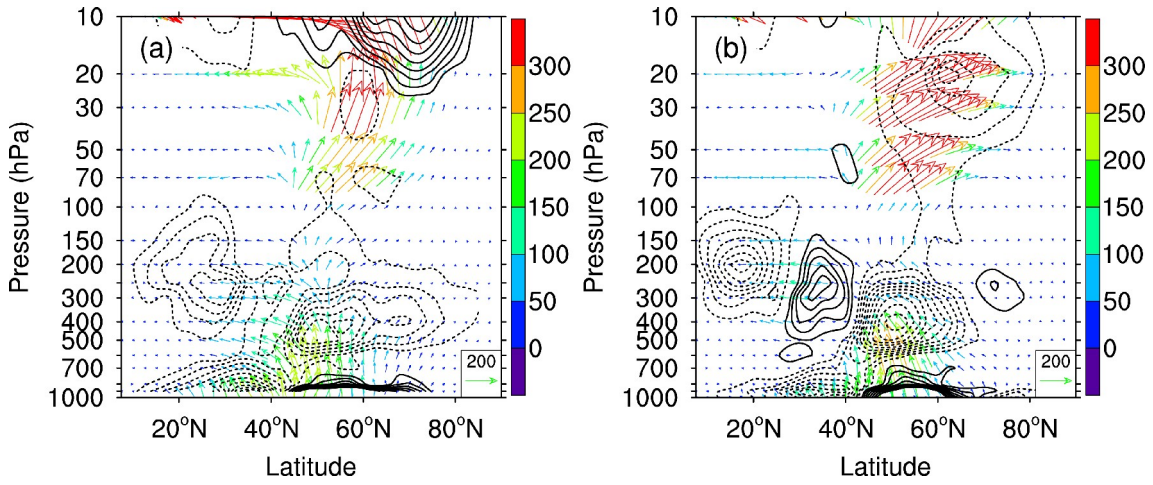

Fig. 4. Height–latitude cross section of the Eliassen–Palm flux (vectors; units: $m^2\ s^{-2}$) and its divergence (contours; interval 100 $m^2\ s^{-2}$) (a) averaged from 28 to 31 December 2020 and (b) averaged from 2 to 5 January 2021. The vectors are scaled by $\sqrt{1000/p}$ at all levels and are magnified by a scale factor of five above 100 hPa for a better visualization of the smaller vectors in the stratosphere. This scaling method is applied after Eq. (3).

positive geopotential anomalies extending from the midstratosphere to the midtroposphere over the Urals–Siberia region at the beginning of January 2021. This suggests that the downward propagation of SSW signal not only enhanced the negative phase of the Arctic Oscillation but also strengthened the Urals–Siberia blocking.

To further investigate the influence of the SSW and the displacement of the stratospheric polar vortex on the atmospheric circulation in the troposphere, we examined the height–latitude cross section of the PV along East Asia and the Arctic (Fig. 6a). The tropopause is generally represented by a set of dense contours at 1.5–3 PVU (Davis and Emanuel, 1991), slopes downward with latitude, and is straight and smooth. The high PV cold air mass (PV > 4 PVU) in the lower stratosphere usually assembles in the Arctic region. On 6 January 2021, a distinct tropopause folding was observed at 100–500 hPa above East Asia (30°–50°N) as a result of the southward shift of the stratospheric polar vortex (Fig. 3e). The high-PV dry and cold air mass originating from the Arctic stratosphere drained into the area of folding and eventually intruded into the mid and lower troposphere over East Asia. The intrusion of this high-PV cold air resulted in the cold wave and snowstorms in East Asia by enhancing the negative geopotential perturbations and cyclonic vorticity (Davis et al., 1996). It can be seen from Fig. 6b that the high-PV air mass extended southward from high latitudes to East Asia at the 315-K isentropic surface, which was accompanied by the southward intrusion of the severe cold air. Since the 315-K isentropic surface slopes downward from north to south in the Northern Hemisphere, the southward intrusion of cold airflow at the 315-K isentropic surface also confirmed that cold air originated from the Arctic region in the lower stratosphere. Yi et al. (2013) investigated the relationship between 17 stratospheric weak polar vortex events and surface temperature variation in winter in East Asia. They found that the cold air with high PV remains near 60°N in the early and middle period of the weak vortex event and begins to extend southward in the late period. In the middle and upper troposphere, cold air from the high latitudes can migrate to 45°N and lower the surface temperature in northern China.

At 500 hPa, the negative phase of the Arctic Oscillation was characterized by a displacement of the tropospheric polar vortex from the pole to the East Asia–North Pacific sector. Meanwhile, two blocking highs became established in the upstream and downstream areas of the displaced vortex and an inverted omega-shaped circulation pattern (IOCP) therefore formed in the region of 40º–80ºN, 90ºE–120ºW (Fig. 7a). Apparently, the blocking high in the downstream area (120ºW) was weaker than the blocking in the Urals–Siberia region. The downward propagating stratospheric signals of strong positive geopotential height anomalies over the polar cap (Fig. 5a) induced the positive geopotential anomaly in the midtroposphere (Fig. 7b) and greatly weakened the tropospheric polar vortex. As a result, the tropospheric polar vortex was shifted off the pole. Besides influence from the stratosphere, Si et al. (2021) found that the occurrence of an IOCP is also a result of the southward shift of the tropospheric polar vortex and the propagation of Rossby wave energy at northern mid-to-high latitudes. Figure 7a shows that the Rossby wave energy propagated eastward along the northern mid-to-high latitudes and was absorbed into the Urals–Siberia region, contributing to the occurrence of the Urals–Siberia blocking. Furthermore, eastward propagating Rossby wave energy was absorbed over western North America in the Western Hemisphere, which favored another downstream blocking ridge in western North America. The IOCP eventually formed in the East Asia–North Pacific region. The high-PV cold air mass was assembled in the IOCP, while a low-PV air mass prevailed outside the IOCP (Fig. 8) where a blocking or anticyclonic circulation dominated (Hoskins et al., 1985). The air with PV

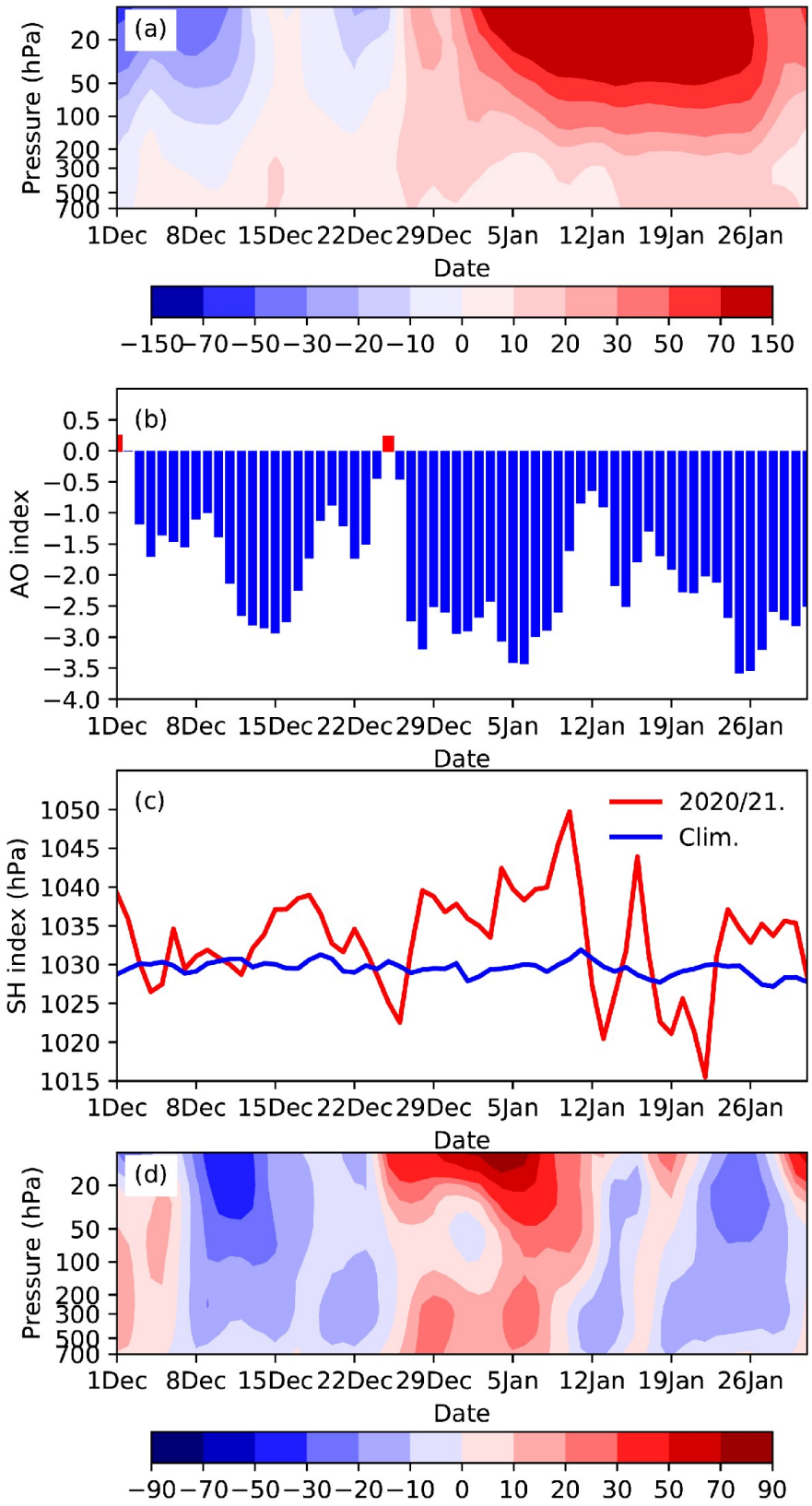

Fig. 5. (a) Time–height cross section of the geopotential height anomaly (units: dagpm) over the polar cap from 1 December 2020 to 31 January 2021. (b) Arctic Oscillation index from 1 December 2020 to 31 January 2021. (c) Siberian high index (units: hPa) from 1 December 2020 to 31 January 2021. The climatological mean period is defined as 1981–2010. (d) Time–height cross section of geopotential height anomaly (units: dagpm) averaged over 55°–75°N, 80°–110°E from 1 December 2020 to 31 January 2021.

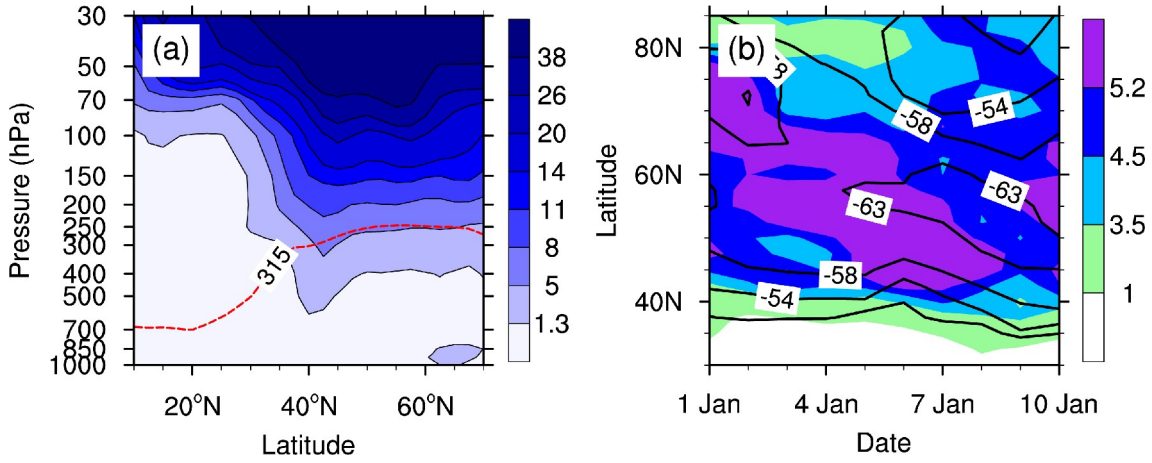

Fig. 6. (a) Height–latitude cross section of the potential vorticity (shading; units: PVU) and 315-K potential temperature contour (red dotted contour; units: K) averaged along 115°–135°E on 6 January 2021. (b) Latitude–time cross section of the potential vorticity (shading; units: PVU) and temperature (contours; units: °C) at the 315-K isentropic surface averaged along 115°–135°E from 1 to 10 January 2021.

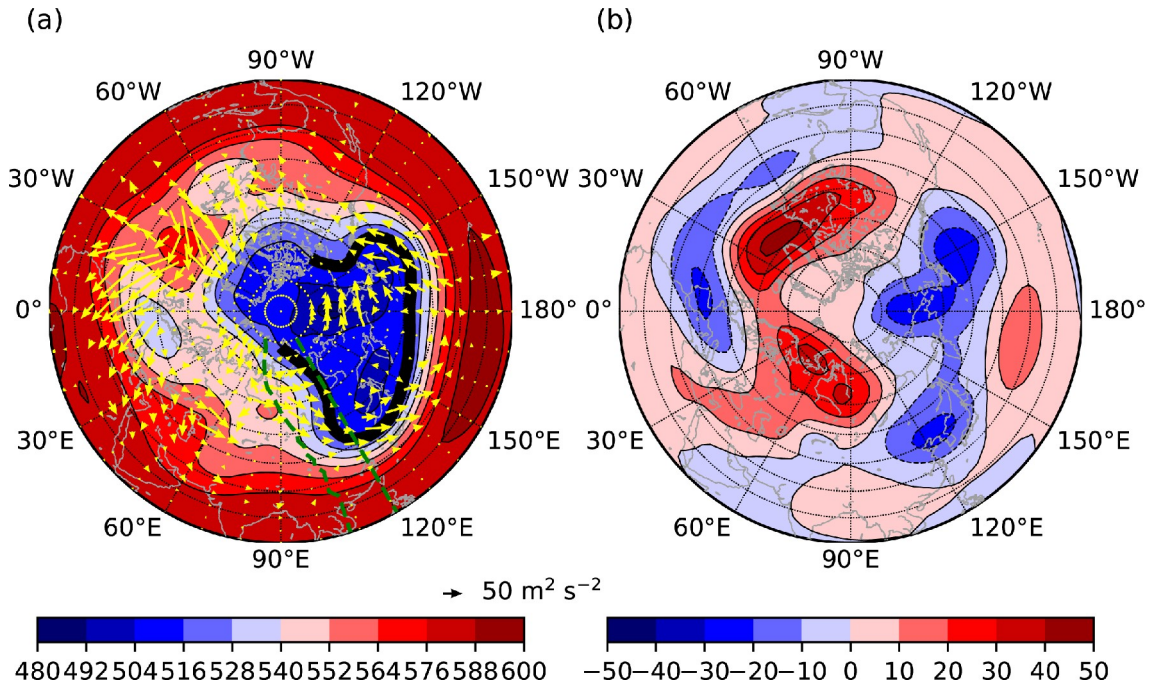

Fig. 7. (a) Geopotential height (shading; units: dagpm) and TN wave activity flux (vectors; units: $m^2\ s^{-2}$) at 500 hPa averaged from 5 to 8 January 2021. The bold black 528-dagpm isoline in the East Asia–North Pacific sector indicates the location of the IOCP. The green dotted lines (the left line: 60°, 67.5°, 70°, 72.5°, 75°, 77.5°, 80°, 85°, 87.5°, 90°, 92.5°, 95°, 97.5°, 97.5°, 100°, 100°, 102.5°, 102.5°, 105°, 105.0°, 105°, 105°, 107.5°, 107.5°, 107.5°, 107.5°, 107.5°, 107.5°, 107.5°E for latitudes from 80°N to 10°N, and the right line: 120°E for latitudes from 80°N to 10°N) indicate the transect location in Fig. 9. (b) Geopotential height anomalies at 500 hPa (shading; units: dagpm) averaged from 5 to 8 January 2021.

values > 5 PVU was mainly concentrated above Siberia, and its temperature was lower than –56ºC. As the IOCP moved southeastward, its southern edge finally reached East Asia, there was an outburst of high-PV cold air, and the cold wave swept through East Asia from 6 to 8 January (Fig. 8).

Figure 9 shows the evolution of the vertical structure of the IOCP averaged between the two green lines in Fig. 7a. The IOCP conveyed the high-PV airflow along isentropic surfaces (between 330–290 K) to East Asia. The increased PV in the mid-to-high troposphere was mainly located at 60°N on 4 January and 40°N on 6 January (left panel in Fig. 9). According to the isentropic PV equation (Hoskins et al., 1985), the PV can be treated as a combined variable of the static stability and absolute vorticity at an isentropic surface. The static stability is lower in the troposphere than in

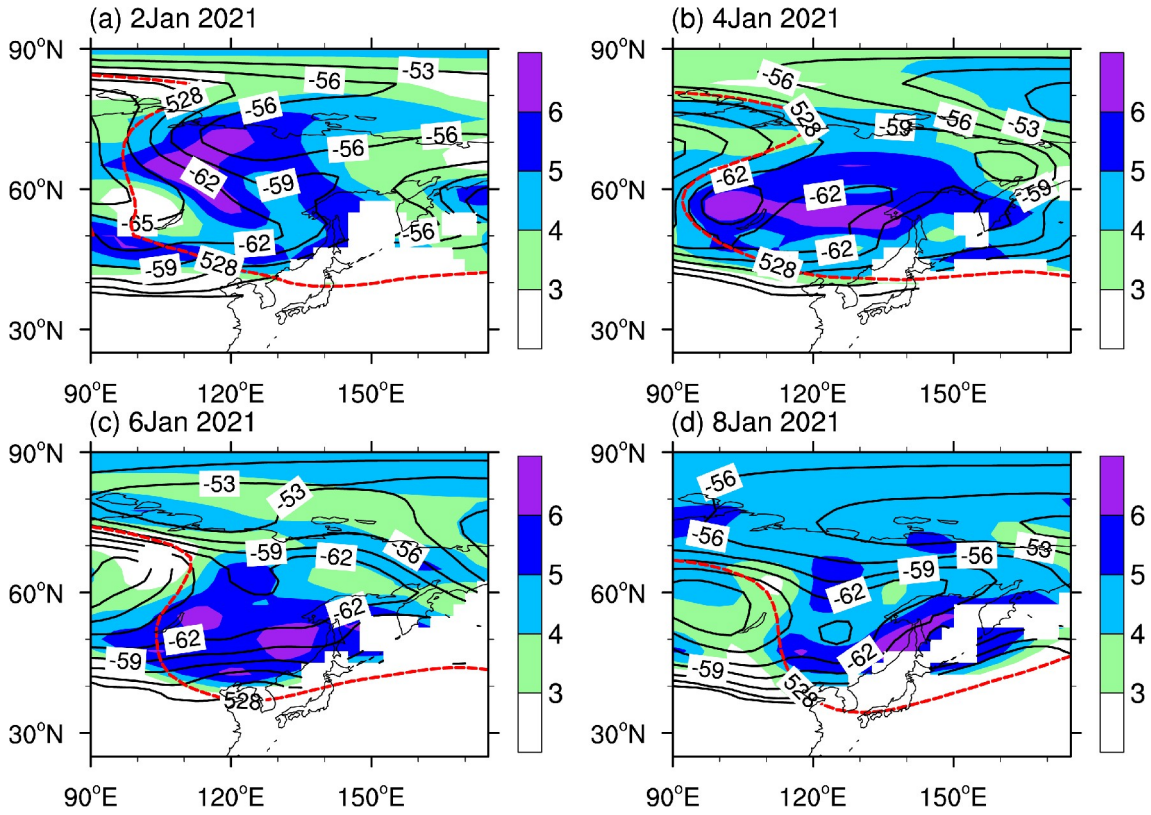

Fig. 8. The potential vorticity (shading; units: PVU), temperature (black contours; units: °C) at the 315-K isentropic surface, and 528 dagpm geopotential height contour at 500 hPa (red dashed contours) on alternate days from 2 to 8 January 2021.

the stratosphere. The absolute vorticity of the air mass therefore increases when moving downward from the stratosphere to the troposphere. Accordingly, the downward intrusion of the high-PV airflow lowered the geopotential height in front of the folding area, which enhanced cyclonic vorticity and upward motion between 25°–30°N (right panel in Fig. 9).

By contrast, the geopotential height and downward motion to the north of the IOCP (Siberian and Arctic regions) increased (right panel in Fig. 9). As seen in Figs. 9d and f, the downward motion was enhanced in the regions north of the IOCP (50°–65°N). Thus, the upward motion in East Asia and downward motion to the north of the IOCP formed a meridional cell extending from East Asia to Siberia. The downward branch brought negative vorticity and anticyclonic advection to Siberia and thus intensified the Siberian high (Fig. 5c), which contributed to the southward outbreak of the cold wave (Si et al., 2021). In the lower troposphere, the northerly wind induced by the meridional cell favored the southward intrusion of the cold wave. These results are consistent with our previous study (Si et al., 2021), which showed that the IOCP induced a meridional cell along the East Asia–Siberia sector that enhanced the Siberian high and contributed to the outbreak of the extreme cold wave in East Asia in January 2016.

4. Summary

An unprecedented cold wave swept through East Asia in early January 2021. The dramatic drops in temperature from 6 to 8 January 2021 either broke records or reached extreme historical values at 383 sites to the north of the Yangtze River in China. A major SSW event occurred before this unprecedented cold wave at the beginning of January 2021. The stratospheric zonal-mean temperature gradient between the Arctic and mid-to-high latitudes reversed on 2 January 2021, and the stratospheric zonal-mean wind at mid-to-high latitudes changed to easterly on 5 January 2021. According to the World Meteorological Organization definition, this SSW event was classified as a major warming event.

The proposed mechanisms for the influences of this major SSW event on the unprecedented cold wave in East Asia in January 2021 are presented in Fig. 10. The SSW event shifted the stratospheric polar vortex off the pole toward northern East Asia. The displaced polar vortex resulted in a distinct tropopause folding and brought a high-PV cold air mass to East Asia along isentropic surfaces between 330–290 K. At the same time, the SSW also induced the stratospheric signal to propagate downward to the troposphere, which not only enhanced the negative phase of the Arctic Oscillation, but also shifted the tropospheric polar vortex off the pole toward East Asia. The associated downward

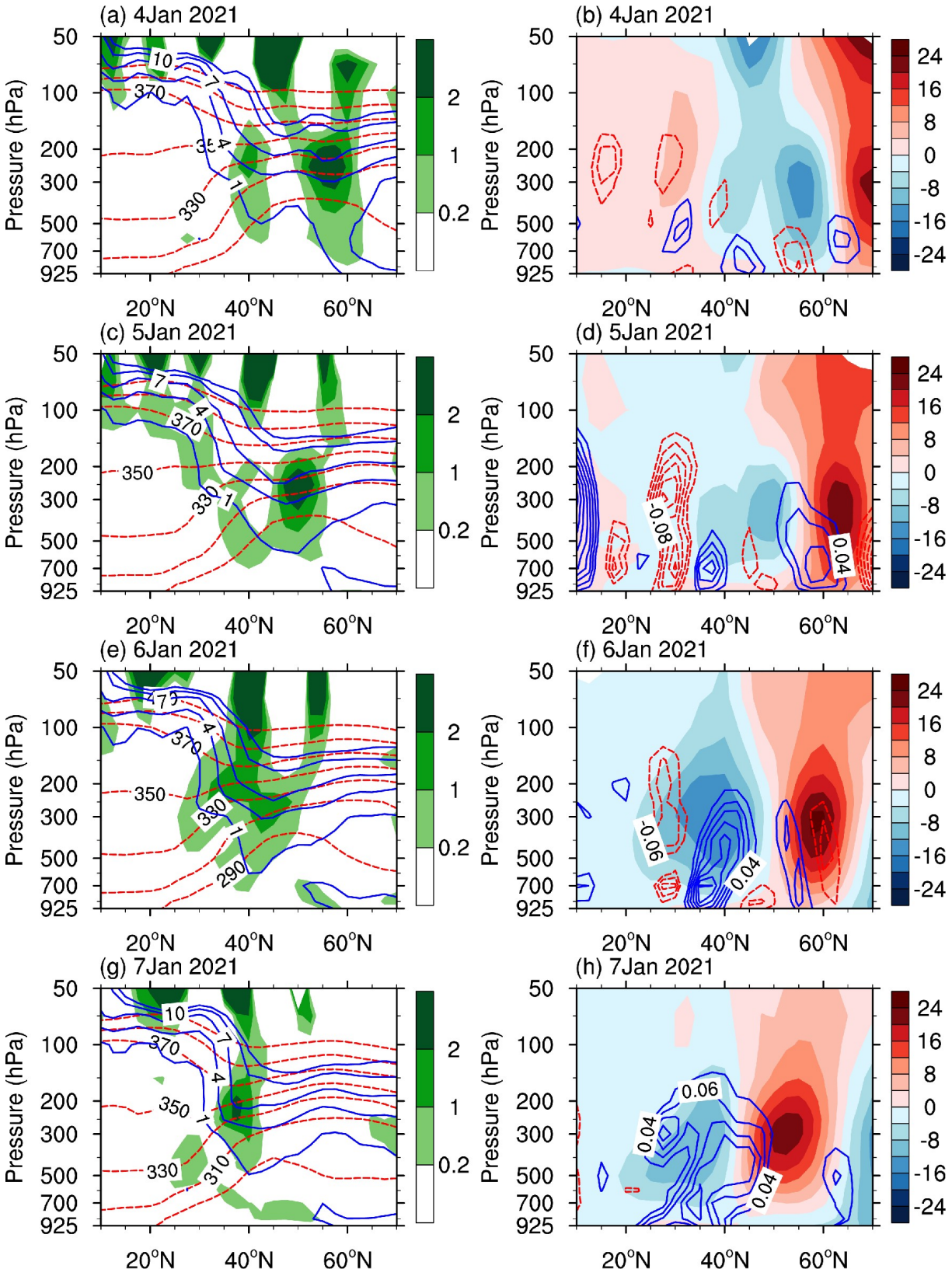

Fig. 9. (Left panel) Height–latitude cross section of the potential temperature (dashed red contours; units: K), potential vorticity (solid blue contours; units: PVU) on the current day, and the change of potential vorticity (shading; units: PVU) between the current day and preceding two days averaged between the two green lines in Fig. 7a from 4 to 7 January 2021. (Right panel) Same as left panel, but for the height–latitude cross section of the change in the geopotential height (shading; units: dagpm) and vertical velocity (contours; units: Pa s^{-1}).

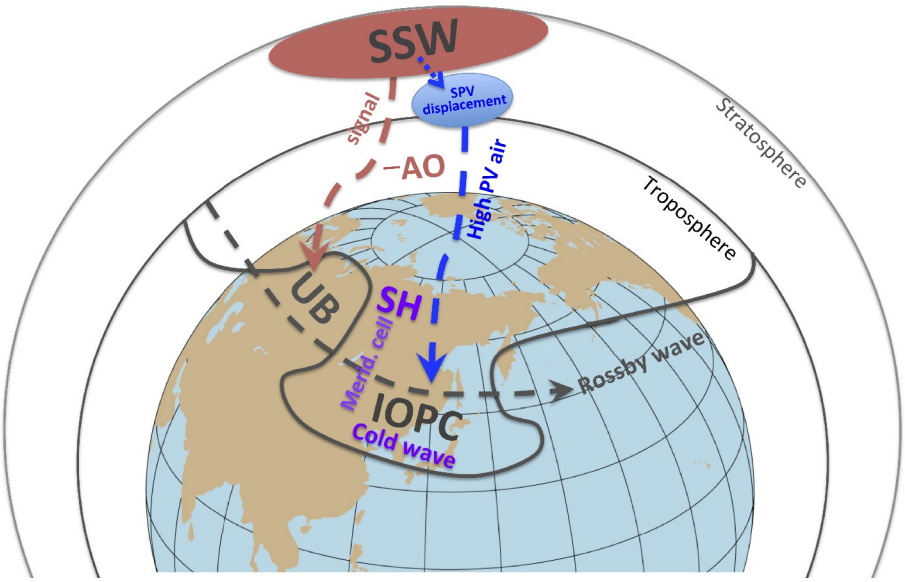

Fig. 10. Schematic diagram of the influence of the major SSW event on the extreme East Asian cold wave in January 2021. SSW, stratospheric sudden warming; SPV, stratospheric polar vortex; AO, Arctic Oscillation; PV, potential vorticity; SH, Siberian high; UB, Ural blocking; Merid., Meridional; IOCP, inverted omega-shaped circulation pattern.

propagation signal also contributed to the blocking high over the Urals–Siberia region. Another blocking ridge occurred over western North America as a result of the eastward propagation of Rossby wave energy. An IOCP eventually formed in the East Asia–North Pacific sector; the IOCP is the most direct and impactful atmospheric pattern causing cold waves in this region. The IOCP triggered a meridional cell with an upward branch in East Asia and a downward branch in Siberia. This meridional cell contributed to a stronger Siberian high and northerly winds in the lower troposphere, which also favored the southward intrusion of the cold wave into East Asia.

Our study emphasizes the unique role of downward propagation of this major SSW on the extreme cold wave in East Asia in early January 2021. The SSW event occurred on 2 January 2021, and the extreme cold wave in China occurred four days later. Hence, SSW may be a good predictand of extreme cold events at northern midlatitudes. The results of this study are consistent with those of our previous study (Si et al., 2021), which shows that the IOCP is the most direct and important atmospheric pattern responsible for extreme cold waves in East Asia in January 2016. The influences of SSW on this extreme cold wave in East Asia have also been confirmed by other studies (Zhang et al., 2021a; Yu et al., 2022). Moreover, the tropospheric dynamics also played an important role in the occurrence of this extreme cold wave. The synergistic effect of the warm Arctic and the cold tropical Pacific in winter 2020/21 is suggested to have been an indispensable background for this cold wave (Zheng et al., 2021). It has also been found that the Ural blocking high, negative phase of the Arctic Oscillation (Bueh et al., 2022; Yao et al., 2022), and enhancement of the Siberian high (Wang et al., 2021) all played important roles. Moreover, the low Arctic sea ice cover is thought to be a precursor signal of this extreme cold wave in East Asia (Dai et al., 2021; Yao et al., 2022).

Acknowledgements. This work was jointly supported by the National Natural Science Foundation of China (Grant Nos. 41790471, 41991284, and 41875104) and the Strategic Priority Research Program of the Chinese Academy of Sciences (Grant No. XDA20100304). The NCL script for calculating the Eliassen–Palm flux was provided by Joe Barsugli from his website at https://psl.noaa.gov/data/epflux/. The Python software for calculating the wave activity flux was provided by Lai Sheng from the website at https://github.com/shuanger1217/T-N_Wave-Activity-Flux. The daily minimum temperatures used in this study, which are derived from the Meteorological Disaster Risk Management System developed by the National Climate Center of the China Meteorological Administration, are available from the China Meteorological Data Service Center (CMDC), National Meteorological Information Center (NMIC) (http://data.cma.cn/en/?r=data/detail&dataCode=SURF_CLI_CHN_MUL_DAY_CES_V3.0).

APPENDIX

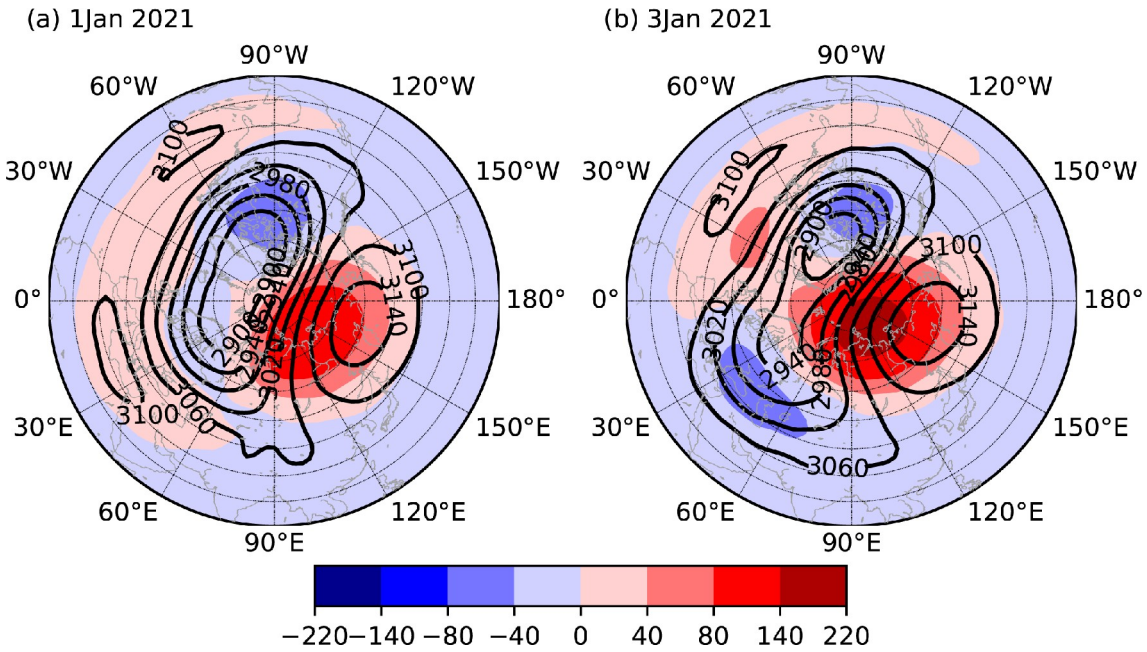

Fig. A1. Geopotential height (contours; units: dagpm) and its anomalies (shading; units: dagpm) at 10 hPa on (a) 1 and (b) 3 January 2021.

REFERENCES

Andrews, D. G., J. R. Holton, and C. B. Leovy, 1987: *Middle Atmosphere Dynamics*. Academic Press, 489 pp.

Bueh, C., J. B. Peng, D. W. Lin, and B. M. Chen, 2022: On the two successive supercold waves straddling the end of 2020 and the beginning of 2021. *Adv. Atmos. Sci.*, https://doi.org/10.1007/s00376-021-1107-x.

Charlton, A. J., and L. M. Polvani, 2007: A new look at stratospheric sudden warmings. *Part I: Climatology and modeling benchmarks. J. Climate*, **20**, 449–469, https://doi.org/10.1175/JCLI3996.1.

Charlton, A. J., A. Oneill, W. A. Lahoz, and A. C. Massacand, 2004: Sensitivity of tropospheric forecasts to stratospheric initial conditions. *Quart. J. Roy. Meteor. Soc.*, **130**, 1771–1792, https://doi.org/10.1256/qj.03.167.

Chen, T.-C., M.-C. Yen, W.-R. Huang, and W. A. Gallus Jr., 2002: An East Asian cold surge: Case study. *Mon. Wea. Rev.*, **130**, 2271–2290, https://doi.org/10.1175/1520-0493(2002)130<2271:AEACSC>2.0.CO;2.

Dai, G. K., and M. Mu, 2020: Arctic influence on the eastern Asian cold surge forecast: A case study of January 2016. *J. Geophys. Res.*, **125**, e2020JD033298, https://doi.org/10.1029/2020jd033298.

Dai, G. K., C. X. Li, Z. Han, D. H. Luo, and Y. Yao, 2021: The nature and predictability of the East Asian extreme cold events of 2020/21. *Adv. Atmos. Sci.*, https://doi.org/10.1007/s00376-021-1057-3.

Davini, P., C. Cagnazzo, and J. A. Anstey, 2014: A blocking view of the stratosphere-troposphere coupling. *J. Geophys. Res.*, **119**, 11 100–11 115, https://doi.org/10.1002/2014jd021703.

Davis, C. A., and K. A. Emanuel, 1991: Potential vorticity diagnostics of cyclogenesis. *Mon. Wea. Rev.*, **119**, 1929–1953, https://doi.org/10.1175/1520-0493(1991)119<1929:PVDOC>2.0.CO;2.

Davis, C. A., E. D. Grell, and M. A. Shapiro, 1996: The balanced dynamical nature of a rapidly intensifying oceanic cyclone. *Mon. Wea. Rev.*, **124**, 3–26, https://doi.org/10.1175/1520-0493(1996)124<0003:tbdnoa>2.0.co;2.

Ding, Y. H., and T. N. Krishnamurti, 1987: Heat budget of the Siberian high and the winter monsoon. *Mon. Wea. Rev.*, **115**, 2428–2449, https://doi.org/10.1175/1520-0493(1987)115<2428:HBOTSH>2.0.CO;2.

Ding, Y. H., and X. Q. Ma, 2008: Analysis of isentropic potential vorticity for a strong cold wave during 2004/2005 winter. *Acta Meteorologica Sinica*, **22**, 129–142.

Ding, Y. H., Z. Y. Wang, Y. F. Song, and J. Zhang, 2008: The unprecedented freezing disaster in January 2008 in southern China and its possible association with the global warming. *Acta Meteorologica Sinica*, **22**, 538–558.

Edmon, H. J. Jr., B. J. Hoskins, and M. E. McIntyre, 1980: Eliassen-Palm cross sections for the troposphere. *J. Atmos. Sci.*, **37**, 2600–2616, https://doi.org/10.1175/1520-0469(1980)037<2600:EPCSFT>2.0.CO;2.

Gillett, N. P., and D. W. J. Thompson, 2003: Simulation of recent Southern Hemisphere climate change. *Science*, **302**, 273–275, https://doi.org/10.1126/science.1087440.

Gong, D.-Y., and C.-H. Ho, 2002: The Siberian high and climate change over middle to high latitude Asia. *Theor. Appl. Climatol.*, **72**, 1–9, https://doi.org/10.1007/s007040200008.

Honda, M., J. Inoue, and S. Yamane, 2009: Influence of low Arctic sea-ice minima on anomalously cold Eurasian winters. *Geophys. Res. Lett.*, **36**, L08707, https://doi.org/10.1029/2008gl037079.

Hori, M. E., J. Inoue, T. Kikuchi, M. Honda, and Y. Tachibana, 2011: Recurrence of intraseasonal cold air outbreak during

the 2009/2010 winter in Japan and its ties to the atmospheric condition over the Barents-Kara Sea. *Sola*, **7**, 25–28, https://doi.org/10.2151/sola.2011-007.

Hoskins, B. J., M. E. McIntyre, and A. W. Robertson, 1985: On the use and significance of isentropic potential vorticity maps. *Quart. J. Roy. Meteor. Soc.*, **111**, 877–946, https://doi.org/10.1002/qj.49711147002.

Jeong, J.-H., and C.-H. Ho, 2005: Changes in occurrence of cold surges over East Asia in association with Arctic Oscillation. *Geophys. Res. Lett.*, **32**, L14704, https://doi.org/10.1029/2005gl023024.

Kalnay, E., and Coauthors, 1996: The NCEP/NCAR 40-year reanalysis project. *Bull. Amer. Meteor. Soc.*, **77**, 437–472, https://doi.org/10.1175/1520-0477(1996)077<0437:TNYRP>2.0.CO;2.

Krüger, K., B. Naujokat, and K. Labitzke, 2005: The unusual midwinter warming in the Southern Hemisphere stratosphere 2002: A comparison to Northern Hemisphere phenomena. *J. Atmos. Sci.*, **62**, 603–613, https://doi.org/10.1175/JAS-3316.1.

Kuang, X. Y., Y. C. Zhang, Z. Y. Wang, D. Q. Huang, and Y. Huang, 2019: Characteristics of boreal winter cluster extreme events of low temperature during recent 35 years and its future projection under different RCP emission scenarios. *Theor. Appl. Climatol.*, **138**, 569–579, https://doi.org/10.1007/s00704-019-02850-8.

Liu, Y., and Y. L. Zhang, 2014: Overview of the major 2012-2013 Northern Hemisphere stratospheric sudden warming: Evolution and its association with surface weather. *Journal of Meteorological Research*, **28**, 561–575, https://doi.org/10.1007/s13351-014-3065-z.

Lu, C. H., and Y. H. Ding, 2013: Observational responses of stratospheric sudden warming to blocking highs and its feedbacks on the troposphere. *Chinese Science Bulletin*, **58**, 1374–1384, https://doi.org/10.1007/s11434-012-5505-4.

Lü, Z. Z., F. Li, Y. J. Orsolini, Y. Q. Gao, and S. P. He, 2020: Understanding of European cold extremes, sudden stratospheric warming, and Siberian snow accumulation in the winter of 2017/18. *J. Climate*, **33**, 527–545, https://doi.org/10.1175/jcli-d-18-0861.1.

Luo, D. H., Y. Q. Xiao, Y. Yao, A. G. Dai, I. Simmonds, and C. L. E. Franzke, 2016: Impact of Ural blocking on winter warm Arctic-cold Eurasian anomalies. *Part I: Blocking-induced amplification. J. Climate*, **29**, 3925–3947, https://doi.org/10.1175/jcli-d-15-0611.1.

Ma, S. M., and C. W. Zhu, 2019: Extreme cold wave over East Asia in January 2016: A possible response to the larger internal atmospheric variability induced by Arctic warming. *J. Climate*, **32**, 1203–1216, https://doi.org/10.1175/jcli-d-18-0234.1.

Matsuno, T., 1971: A dynamical model of the stratospheric sudden warming. *J. Atmos. Sci.*, **28**, 1479–1494, https://doi.org/10.1175/1520-0469(1971)028<1479:ADMOTS>2.0.CO;2.

Mitchell, D. M., L. J. Gray, J. Anstey, M. P. Baldwin, and A. J. Charlton-Perez, 2013: The influence of stratospheric vortex displacements and splits on surface climate. *J. Climatol.*, **26**, 2668–2682, https://doi.org/10.1175/JCLI-D-12-00030.1.

Nakagawa, K. I., and K. Yamazaki, 2006: What kind of stratospheric sudden warming propagates to the troposphere. *Geophys. Res. Lett.*, **33**, L04801, https://doi.org/10.1029/2005gl024784.

Overland, J. E., K. R. Wood, and M. Y. Wang, 2011: Warm Arctic-cold continents: Climate impacts of the newly open Arctic Sea. *Polar Research*, **30**, 15787, https://doi.org/10.3402/polar.v30i0.15787.

Park, T.-W., J.-H. Jeong, C.-H. Ho, and S.-J. Kim, 2008: Characteristics of atmospheric circulation associated with cold surge occurrences in East Asia: A case study during 2005/06 winter. *Adv. Atmos. Sci.*, **25**, 791–804, https://doi.org/10.1007/s00376-008-0791-0.

Petoukhov, V., and V. A. Semenov, 2010: A link between reduced Barents-Kara sea ice and cold winter extremes over northern continents. *J. Geophys. Res*, **115**, D21111, https://doi.org/10.1029/2009jd013568.

Ren, F. M., and Coauthors, 2012: An objective identification technique for regional extreme events. *J. Climate*, **25**, 7015–7027, https://doi.org/10.1175/Jcli-D-11-00489.1.

Scaife, A. A., and J. R. Knight, 2008: Ensemble simulations of the cold European winter of 2005–2006. *Quart. J. Roy. Meteor. Soc.*, **134**, 1647–1659, https://doi.org/10.1002/qj.312.

Si, D., Y. H. Ding, and D. B. Jiang, 2021: A low-frequency downstream development process leading to the outbreak of a mega-cold wave event in East Asia. *J. Meteor. Soc. Japan*, **99**, 1185–1200, https://doi.org/10.2151/jmsj.2021-058.

Takaya, K., and H. Nakamura, 2001: A formulation of a phase-independent wave-activity flux for stationary and migratory quasigeostrophic eddies on a zonally varying basic flow. *J. Atmos. Sci.*, **58**, 608–627, https://doi.org/10.1175/1520-0469(2001)058<0608:afoapi>2.0.co;2.

Takaya, K., and H. Nakamura, 2005a: Mechanisms of intraseasonal amplification of the cold Siberian high. *J. Atmos. Sci.*, **62**, 4423–4440, https://doi.org/10.1175/jas3629.1.

Takaya, K., and H. Nakamura, 2005b: Geographical dependence of upper-level blocking formation associated with intraseasonal amplification of the Siberian high. *J. Atmos. Sci.*, **62**, 4441–4449, https://doi.org/10.1175/JAS3628.1.

Tao, S.-Y., 1957: A synoptic and aerological study on a cold wave in the far East during the period of the break down of the blocking situation over Euroasia and Atlantic. *Acta Meteorologica Sinica*, **28**, 63–74, https://doi.org/10.11676/qxxb1957.005. (in Chinese with English abstract)

Tao, S.-Y., and J. Wei, 2008: Severe snow and freezing-rain in January 2008 in the southern China. *Climatic and Environmental Research*, **13**, 337–350, https://doi.org/10.3878/j.issn.1006-9585.2008.04.01. (in Chinese with English abstract)

Thompson, D. W. J., and J. M. Wallace, 1998: The Arctic Oscillation signature in the wintertime geopotential height and temperature fields. *Geophys. Res. Lett.*, **25**, 1297–1300, https://doi.org/10.1029/98gl00950.

Tomassini, L., E. P. Gerber, M. P. Baldwin, F. Bunzel, and M. Giorgetta, 2012: The role of stratosphere-troposphere coupling in the occurrence of extreme winter cold spells over northern Europe. *Journal of Advances in Modeling Earth Systems*, **4**, M00A03, https://doi.org/10.1029/2012ms000177.

Wang, C. Z., Y. L. Yao, H. L. Wang, X. B. Sun, and J. Y. Zheng, 2021: The 2020 summer floods and 2020/21 winter extreme cold surges in China and the 2020 typhoon season in the western North Pacific. *Adv. Atmos. Sci.*, **38**, 896–904, https://doi.org/10.1007/s00376-021-1094-y.

Wang, L., and W. Chen, 2010: Downward Arctic Oscillation signal associated with moderate weak stratospheric polar vortex and the cold December 2009. *Geophys. Res. Lett.*, **37**,

L09707, https://doi.org/10.1029/2010gl042659.

Wen, M., S. Yang, A. Kumar, and P. Q. Zhang, 2009: An analysis of the large-scale climate anomalies associated with the snowstorms affecting China in January 2008. *Mon. Wea. Rev.*, **137**, 1111–1131, https://doi.org/10.1175/2008mwr2638.1.

Wu, B. Y., J. Z. Su, and R. D'Arrigo, 2015: Patterns of Asian winter climate variability and links to Arctic sea ice. *J. Climate*, **28**, 6841–6858, https://doi.org/10.1175/jcli-d-14-00274.1.

Wu, B. Y., K. Yang, and J. A. Francis, 2017: A cold event in Asia during January-February 2012 and its possible association with Arctic sea ice loss. *J. Climate*, **30**, 7971–7990, https://doi.org/10.1175/jcli-d-16-0115.1.

Wu, Z. W., J. P. Li, Z. H. Jiang, and J. H. He, 2011: Predictable climate dynamics of abnormal East Asian winter monsoon: Once-in-a-century snowstorms in 2007/2008 winter. *Climate Dyn.*, **37**, 1661–1669, https://doi.org/10.1007/s00382-010-0938-4.

Yao, Y., W. Q. Zhang, D. H. Luo, L. H. Zhong, and L. Pei, 2022: Seasonal cumulative effect of Ural blocking episodes on the frequent cold events in China during the early winter of 2020/21. *Adv. Atmos. Sci.*, https://doi.org/10.1007/s00376-021-1100-4.

Yi, M. J., Y. J. Chen, R. J. Zhou, Y. Bi, and S. M. Deng, 2013: Relationship between winter surface temperature variation in eastern Asia and stratospheric weak polar vortex. *Chinese Journal of Atmospheric Sciences*, **37**, 668–678, https://doi.org/10.3878/j.issn.1006-9895.2012.12032. (in Chinese with English abstract)

Yu, Y. Y., M. Cai, R. C. Ren, and J. Rao, 2018: A closer look at the relationships between meridional mass circulation pulses in the stratosphere and cold air outbreak patterns in northern hemispheric winter. *Climate Dyn.*, **51**, 3125–3143, https://doi.org/10.1007/s00382-018-4069-7.

Yu, Y. Y., Y. F. Li, R. C. Ren, M. Cai, Z. Guan, and W. Huang, 2022: An isentropic mass circulation view on the extreme cold events in the 2020/21 winter. *Adv. Atmos. Sci.*, https://doi.org/10.1007/s00376-021-1289-2.

Zhang, X. D., and Coauthors, 2021a: Extreme cold events from East Asia to north America in winter 2020/21: Comparisons, causes, and future implications. *Adv. Atmos. Sci.*, https://doi.org/10.1007/s00376-021-1229-1.

Zhang, Y.-X., Y.-J. Liu, and Y.-H. Ding, 2021b: Identification of winter long-lasting regional extreme low-temperature events in Eurasia and their variation during 1948-2017. *Adv. Clim. Change Res.*, **12**, 353–362, https://doi.org/10.1016/j.accre.2021.05.005.

Zheng, F., and Coauthors, 2021: The 2020/21 extremely cold winter in China influenced by the synergistic effect of La Niña and warm Arctic. *Adv. Atmos. Sci.*, https://doi.org/10.1007/s00376-021-1033-y.

Zhou, B. Z., and Coauthors, 2011: The great 2008 Chinese ice storm: Its socioeconomic-ecological impact and sustainability lessons learned. *Bull. Amer. Meteor. Soc.*, **92**, 47–60, https://doi.org/10.1175/2010bams2857.1.

Zhou, W., J. C. L. Chan, W. Chen, J. Ling, J. G. Pinto, and Y. P. Shao, 2009: Synoptic-scale controls of persistent low temperature and icy weather over southern China in January 2008. *Mon. Wea. Rev.*, **137**, 3978–3991, https://doi.org/10.1175/2009mwr2952.1.

Zuo, Z. Y., R. H. Zhang, Y. Huang, D. Xiao, and D. Guo, 2015: Extreme cold and warm events over China in wintertime. *International Journal of Climatology*, **35**, 3568–3581, https://doi.org/10.1002/joc.4229.